Solution Structure of Ptu1, a Toxin from the Assassin Bug *Peirates turpis* That Blocks the Voltage-Sensitive Calcium Channel N-Type†

Cédric Bernard,§ Gerardo Corzo,|| Amor Mosbah,§ Terumi Nakajima,|| and Hervé Darbon*,§

Architecture et Fonction des Macromolécules Biologiques, UMR 6098, CNRS and Universités d'Aix-Marseille I and II, 31 Chemin Joseph Aiguier, 13402 Marseille Cedex 20, France, and Suntory Institute for Bioorganic Research, Mishima-Gun, Shimamoto-Cho, Wakayamadai 1-1-1, Osaka 618-8503, Japan

Received April 26, 2001; Revised Manuscript Received August 17, 2001

ABSTRACT: Ptu1 is a toxin from the assassin bug *Peirates turpis* which has been demonstrated to bind reversibly the N-type calcium channels and to have lower affinity than the ω-conotoxin MVIIA. We have determined the solution structure of Ptu1 by use of conventional two-dimensional NMR techniques followed by distance-geometry and molecular dynamics. The calculated structure of Ptu1 belongs to the inhibitory cystin knot structural family (ICK) that consists of a compact disulfide-bonded core from which four loops emerge. Analysis of the 25 converged solutions indicates that the molecular structure of Ptu1 contains a 2-stranded antiparallel β-sheet (residues 24−27 and 31−34) as the only secondary structure. The loop 2 that has been described to be critical for the binding of the toxin on the channel is similar in Ptu1 and MVIIA. In this loop, the critical residue, Tyr13, in MVIIA is retrieved in Ptu1 as Phe13, but the presence of an acidic residue (Asp16) in Ptu1 could disturb the binding of Ptu1 on the channel and could explain the lower affinity of Ptu1 toward the N-type calcium channel compared to the one of MVIIA. Analysis of the electrostatic charge's repartition gives some insights about the importance of the basic residues, which could interact with acidic residues of the channel and then provide a stabilization of the toxin on the channel.

Numerous small proteins that are natural ligands for ion channels have been described so far. Most of them have been purified from the venom of venomous animals including snakes, scorpions, spiders, bees, and marine cone snails, and their targets are channels specific for sodium, potassium, calcium, or chloride ions. Besides these venomous animals, assassin bugs (Arthropoda: Insecta: Hemiptera: Reduviidae) have been described which are devoid of venom but which produce a toxic saliva. The saliva contains a complex mixture of proteins that are used by the bug either to immobilize the pray or to digest it. One of these small proteins, namely, Ptu1, has been recently purified from the saliva of *Peirates turpis* and chemically and pharmacologically characterized (*1*). Ptu1 has been demonstrated to block reversibly the N-type calcium channels expressed in BHK[1] cells and to be less specific for the L- or P/Q-type calcium channels expressed in similar cell lines. This small protein is 34 amino acid residues long, is cross-linked by 3 disulfide bridges, and has a light sequence homology with conotoxins GVIA and MVIIA (respectively 17% and 23% homologies if Cys residues are omitted because they are not functional residues). The similarity in pharmacological activity of Ptu1 and conotoxins GVIA and MVIIA together with their light sequence homologies encouraged us to determine the solution structure of Ptu1 in order to get insight in the structure−activity relationships of these calcium channel blockers.

MATERIALS AND METHODS

Sample Preparation. Purified Ptu1 (6 mg) has been solubilized in 450 μL of a mixture of H_2O and D_2O in a 9:1 ratio (v/v), leading to a protein concentration of 3.7 mM. The final pH of the Ptu1 solution was 3.0. The amide proton exchange rate was determined after lyophilization of this sample and dissolution in 100% D_2O.

NMR Experiments. All ^{1}H NMR spectra were recorded on a BRUKER DRX500 spectrometer equipped with an HCN probe, and self-shielded triple axis gradients were used. The experiments were performed at two different temperatures in order to solve assignment ambiguities (283 and 300 K). Two-dimensional spectra were acquired using the states-TPPI method (*2*) to achieve F1 quadrature detection (*3*). Water suppression was achieved using presaturation during the relaxation delay (1.5 s), and during the mixing time in the case of NOESY (*4*) experiments, or using a Watergate 3-9-19 pulse train (*5*, *6*) using a gradient at the magic angle obtained by applying simultaneous *x*-, *y*-, and *z*-gradients prior to detection. NOESY spectra were acquired using

† C.B. is supported by the Ministère de l'Education Nationale, de la Recherche et des Techniques. A.M. is supported by a grant from the Centre National de la Recherche Scientifique.

‡ The pdb coordinate files are available on the Brookhaven Data Bank (PDB identification code 1I26).

* To whom correspondence should be addressed at AFMB-UMR 6098, CNRS and Universités d'Aix-Marseille I and II, IFR1, 31, Chemin Joseph-Aiguier, 13402 Marseille CEDEX 20, France. Tel: (33) 91-16-45-35, Fax: (33) 91-16-45-36. E-Mail: herve@afmb.cnrs-mrs.fr.

§ CNRS and Universités d'Aix-Marseille I and II.

|| Suntory Institute for Bioorganic Research.

[1] Abbreviations: BHK, baby hamster kidney; NOESY, nuclear Overhauser effect spectroscopy; TOCSY, total correlation spectroscopy; COSY, correlation spectroscopy; CNS, crystallography and NMR system; ICK, inhibitor cystin knot; CD, circular dichroism.

10.1021/bi015537j CCC: $20.00
Published on Web 10/02/2001

Table 1: Chemical Shifts of Ptu1 at 300 K[a]

residue	HN	H^{α}	H^{β}	other
A1		4.06	1.49	
E2	8.75	4.36	2.06,1.95	$C^{\gamma}H_2$ 2.44
K3	8.62	4.33	1.83,1.75	$C^{\gamma}H_2$ 1.38; $C^{\delta}H_2$ 1.66; $C^{\epsilon}H_2$ 2.94; $N^{\epsilon}H_2$ 7.56
D4	8.64	4.66	2.85,2.79	
C5	7.80	5.02	2.88,2.75	
I6	9.18	4.10	2.03	$C^{\gamma}H_1$ 0.84,*; $C^{\delta}H_2$ 1.21,1.08; $C^{\delta}H_3$ 0.70
A7	8.85	4.19	1.37	
P8		4.39	2.31,2.10	$C^{\gamma}H_2$ 1.82,*; $C^{\delta}H_2$ 3.70,3.58
G9	9.48	3.99,3.41		
A10	7.356	4.72	1.40	
P11		4.67		$C^{\gamma}H_2$ 2.04,1.92; $C^{\delta}H_2$ 3.79,3.60
C12	7.34	5.01	3.45,2.81	
F13	9.83	4.23	2.99,2.90	$C^{\zeta}1H$ 7.12; $C^{\zeta}H$ 7.41
G14	8.56	3.76,3.36		
T15	7.25	4.05	4.09	$C^{\gamma}H_2$ 1.03
D16	8.93	4.36	3.06,2.80	
K17	7.38	4.66	1.51,*	$C^{\gamma}H_2$ 1.24,*; $C^{\delta}H_2$ 1.37,*; $C^{\epsilon}H_2$ 2.89,*; $N^{\zeta}H_2$ 7.52
P18		4.52		$C^{\gamma}H_2$ 1.94,1.76; $C^{\delta}{}_{H2}$ 3.77,3.63
C19	8.86	4.57	3.22,2.77	
C20	9.38	4.21	3.12,2.49	
N21	8.40	4.81	2.78,2.67	$N^{\delta}H_2$ 7.71,7.08
P22		4.48	2.30,*	$C^{\gamma}H_2$ 1.89,*; $C^{\delta}H_2$ 4.07,3.83
R23	7.90	4.28	1.63,*	$C^{\gamma}H_2$ 2.04,*; $C^{\delta}H_2$ 3.21,*; $N^{\delta}H_2$ 7.28
A24	7.65	4.68	1.17	
W25	8.50	4.85	3.22,3.11	$C^{\delta}H_1$ 7.16; $C^{\epsilon}H_3$ 7.58; $C^{\eta}H_2$ 7.47; $C^{\zeta}H_2$ 7.25; $C^{\zeta}H_3$ 7.17; $N^{\epsilon}H_1$ 10.12
C26	9.27	4.54	3.05,2.86	
S27	8.43	4.78	4.00,3.97	
S28	9.30	3.97	3.72,3.56	
Y29	7.79	4.29	3.02,2.84	$C^{\delta}H$ 7.06; $C^{Z}H$ 6.80
A30	7.73	4.17	1.32	
N31	8.29	4.47	3.29,2.34	$N^{\delta}H_2$ 7.51,7.22
K32	7.11	4.46	1.85,1.33	$C^{\gamma}H$ 1.18,1.07; $C^{\delta}H$ 1.57,1.50; $C^{\epsilon}H_2$ 2.89,*
C33	9.67	4.65	3.09,2.62	
L34	8.64	4.51	1.52,1.73	$C^{\gamma}H$ 1.36; $C^{\delta 1}H_2$ 0.83; $C^{\delta}H_2$ 0.79

[a] (*): resonances that cannot be observed.

mixing times of 100 and 120 ms. TOCSY (*7*, *8*) was performed with a spin locking field strength of 8 kHz and mixing time of 80 ms. The amide proton exchange experiments were recorded immediately after dissolution of the peptides in D_2O. A series of TOCSY spectra with a mixing time of 80 ms were recorded at 283 K, the first one for 1 h, followed by spectra of 4 h each.

Analysis of Spectra. The identification of amino acid spin systems and the sequential assignment were done using the standard strategy described by Wüthrich (*9*), applied with a graphical software, XEASY (*10*). The comparative analysis of TOCSY spectra recorded in water gave the spin system signatures of the protein. The spin systems were then sequentially connected using the NOESY spectra.

Experimental Restraints. The integration of NOE data was done by measuring the peak volumes. These volumes were then translated into upper limit distances by the CALIBA routine of DIANA software (*11*). The lower limit was systematically set at 0.18 nm.

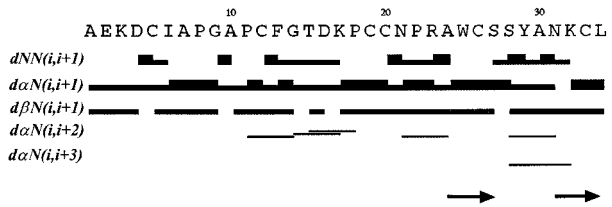

FIGURE 1: Sequence of Ptu1 and sequential assignment. Collected sequential NOEs are classified into strong and weak NOEs and are indicated by thick and thin bars, respectively. The secondary elements (β-sheets) are indicated by arrows.

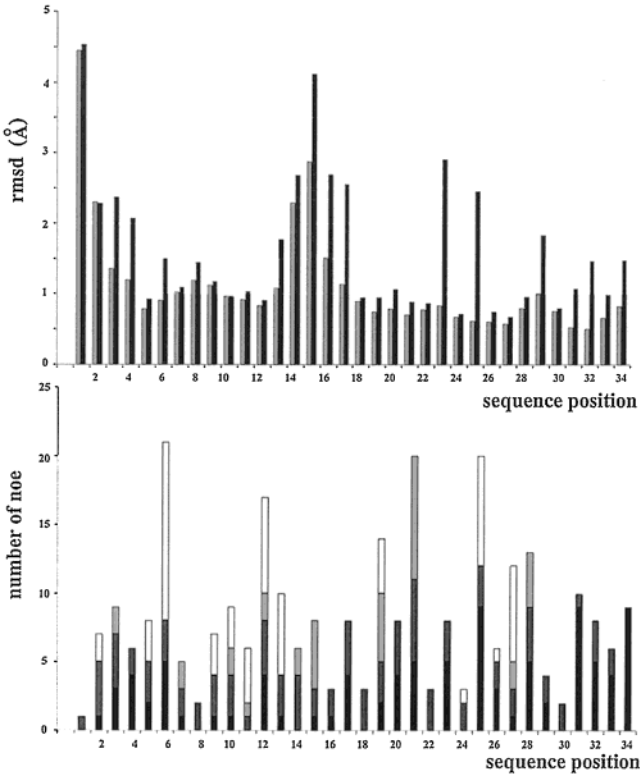

FIGURE 2: RMSD (top) and NOE (bottom) distribution vs sequence. RMSD values for backbone atoms and for all heavy atoms are in gray and black, respectively. Intraresidue NOEs are in black, sequential NOEs are in dark gray, medium-range NOEs are in light gray, and long-range NOEs are in white.

The ϕ torsion angle constraints resulted from the $^3J_{HN-H\alpha}$ coupling constant measurements. They were estimated by the INFIT program (*12*). For a given residue, separated NOESY cross-peaks with the backbone amide proton in the $\varpi 2$ dimension were used. Several cross sections through these cross-peaks were selected that exhibit a good signal-to-noise ratio. They were added up, and only those data points of the peak region that were above the noise level were retained. The left and right ends of the peak region were then brought to zero intensity by a linear baseline correction. After extending the baseline-corrected peak region with zeros on both sides, which is equivalent to oversampling in the time domain, an inverse Fourier transformation was performed. The value of the $^3J_{HN-H\alpha}$ coupling constant was obtained from the first local minimum. $^3J_{HN-H\alpha}$ coupling constants were translated into angle restraints using HABAS from the DIANA package.

Structure Calculation. Distance geometry calculations were performed with the variable target function program DIANA 2.8. A preliminary set of 1000 structures was

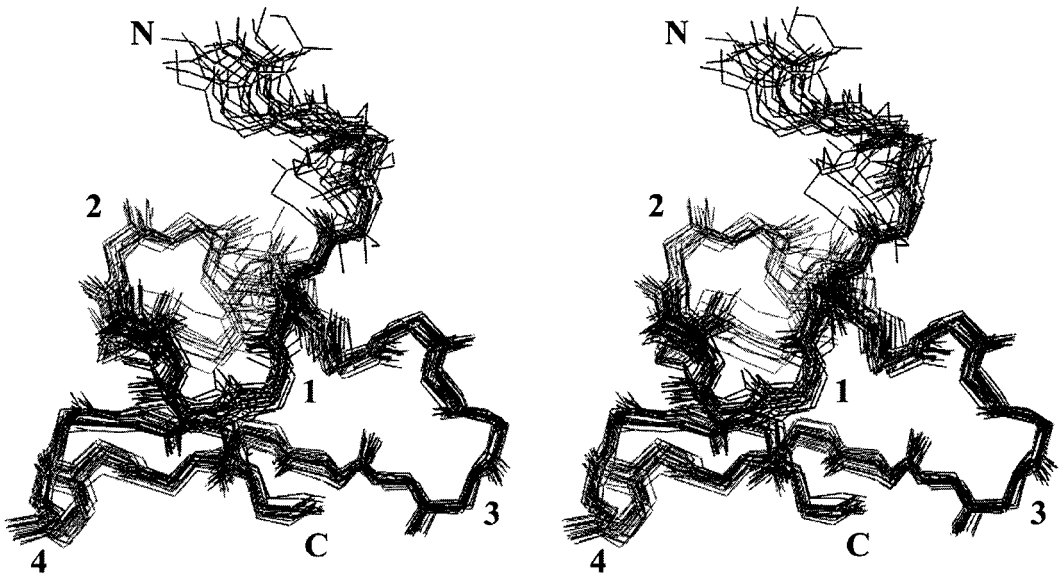

FIGURE 3: Stereoview of the best fit of 25 solution structures of Ptu1. Backbone atoms are shown. The N- and C-terminii are labeled (N and C), and the four loops are indicated by the corresponding number (1, 2, 3, and 4).

Table 2: Global (All Structures) and Partial (Conformations A and B) Root Mean Square Deviations (in Å)

rmsd (Å)		whole sequence	sequence 5−34	sequences 5−13, 18−34
all structures	backbone atoms	1.48 ± 0.51	0.94 ± 0.33	0.62 ± 0.14
	all heavy atoms	2.03 ± 0.40	1.71 ± 0.39	1.35 ± 0.27
conformation A	backbone atoms		0.59 ± 0.17	
	all heavy atoms		1.57 ± 0.21	
conformation B	backbone atoms		0.67 ± 0.19	
	all heavy atoms		1.45 ± 0.26	

Table 3: Structural Statistics of the 25 Best Structures Obtained by Distance Geometry and Minimization

energies (kcal/mol)	total	65.19 ± 8.10
	bonds	3.13 ± 0.45
	angles	26.21 ± 2.00
	impropers	1.57 ± 0.34
	van der Waals (repel)	17.16 ± 4.39
	NOE	16.96 ± 2.68
	cdih	0.17 ± 0.15
rmsd	bonds	$(2.5 \times 10^{-3}) \pm (1.8 \times 10^{-4})$
	angles	$(0.43 \pm 1.67) \times 10^{-2}$
	impropers	$(0.199 \pm 2.11) \times 10^{-2}$
	dihedral	30.58 ± 1.691
	NOE	$(2.82 \times 10^{-2}) \pm (2.2 \times 10^{-3})$
	cdih	$(0.24 \pm 9.9) \times 10^{-2}$

initiated including only intraresidual and sequential upper limit distances. From these, the 500 best structures were kept for a second round, including medium-range distances, and the resulting 250 best structures for a third round, with the whole set of upper limit restraints, and some additional distance restraints, used to define the disulfide bridges (i.e., $d_{S\gamma,S\gamma}$, 0.21 nm; $d_{C\beta,S\gamma}$ and $d_{S\gamma,C\beta}$, 0.31 nm). Starting from the 50 best structures, a REDAC strategy (*11*) was used in a last step, to include the dihedral constraints together with the additional distance restraints coming from hydrogen bonds.

To remove residual bad van der Waals contacts, these 50 structures were refined by restrained molecular dynamics annealing, slow cooling, and energy minimization (parameter file: protein-allhdg in CNS).

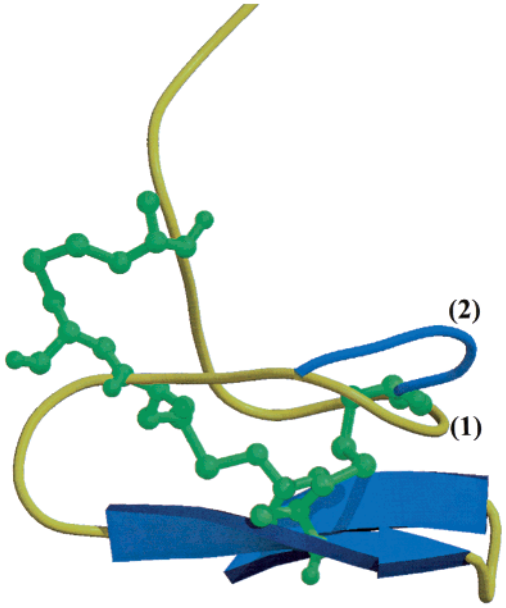

FIGURE 4: Molscript representation (*26*). The two conformations of the 13−18 loop are shown in yellow (1) and blue (2).

The visual analysis was done using the TURBO software, and the geometric quality of the obtained structures was assessed by PROCHECK 3.3 and PROCHECK−NMR software (*13*).

RESULTS AND DISCUSSION

NMR Resonance Assignment. Sequential assignment was obtained by the now standard method first described by Wüthrich (*9*) and successfully applied to various animal toxins (*14, 15*). The spin systems were identified on the basis of both COSY and TOCSY spectra, recorded at 300 and 283 K. The use of two temperatures for recording allowed us to resolve overlapping signals in the fingerprint region, and, thus, intraresidue HN−Hα cross-peaks were unambiguously assigned. At the end of the sequential assignment procedure, almost all protons were identified, and their resonance frequency was determined (Table 1).

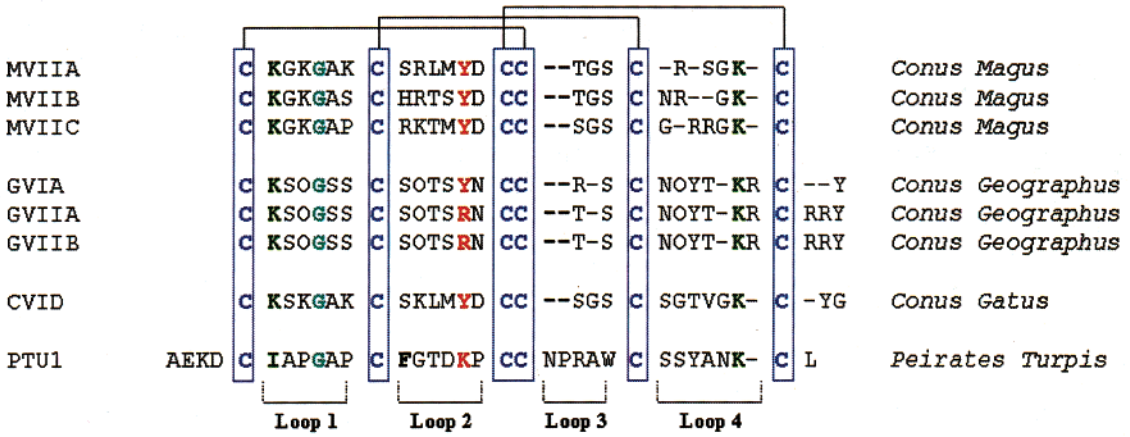

FIGURE 5: Comparison of the sequence of Ptu1 with those of related toxins

Figure 1 represents the result of the sequential correlations found on the NOESY spectrum. As shown by the repartition of the α/H_N and H_N/H_N correlations, the toxin is essentially organized in random coil. However, strong α/H_N correlations indicate that some extended regions are present.

Structure Calculation. The structure of Ptu1 was determined by using 241 NOE-based distance restraints, including 92 intraresidue restraints, 92 sequential restraints, 20 medium-range restraints, and 37 long-range restraints. The repartition of these NOE along the sequence is shown in Figure 2. In addition, 30 hydrogen bond restraints and 21 dihedral angle constraints deriving respectively from proton exchange and coupling constants have been included, as well as 9 distance restraints derived from the 3 disulfide bridges which have been experimentally characterized (*1*). Altogether, the final experimental set corresponded to 8.9 constraints per residue on average (Figure 2). The structures were calculated by using the distance geometry protocol using DIANA and energy-minimized by CNS. The best-fit superimposition of backbone atoms for the 25 best structures gives RMSD values of 1.48 ± 0.51 Å for backbone atoms and 2.03 ± 0.40 Å if all non-hydrogen atoms are included. These quite high values are explained by the existence of a structurally undefined N-terminus and a double conformation for the region encompassing residues 13−17 (loop 2). A summary of the structural statistics and the values of RMSD calculated on the well-defined regions are given in Table 2. All the solutions have good nonbonded contacts, and good covalent geometry was evidenced by low values of CNS energy terms and low RMSD values for bond lengths, valence angles, and improper dihedral angles (Table 3). The correlation with the experimental data shows no NOE-derived distance violation greater than 0.2 Å. The analysis of the Ramachandran plot shows for the ensemble of the 25 calculated models (in PROCHECK software nomenclature) 98.6% of the residues in the most favored and in the additional regions, 1.4% in the generously allowed regions, and none in the disallowed regions (data not shown).

Structure Description. The three-dimensional structure of Ptu1 (PDB id: 1I26) consists of a compact disulfide-bonded core, from which four loops emerge (i.e., loop 1 from Ile6 to Thr11, loop 2 from Phe13 to Pro18, loop 3 from Asn21 to Trp25, and loop 4 from Ser27 to Lys32) as well as N- and C-termini. Figure 3 shows a stereopair representation of the best-fit superposition of the backbone atoms (N, C_α, C) for 25 converged structures. Analysis of the 25 converged

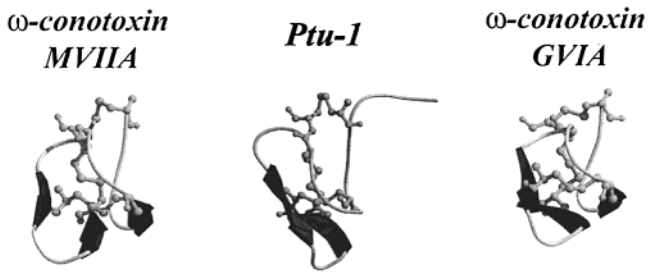

FIGURE 6: Comparison of three-dimensional structures of structurally related toxins with Ptu1 in Molscript representation.

structures indicates that the molecular structure of Ptu1 contains a β-sheet region made of 2 antiparallel β-strands, i.e., β-strand 1 (Ala24 to Ser27) and β-strand 2 (Lys31 to Leu34). No other regular secondary structure can be described. The stretch encompassing residues 13−18 appears to be floppy when only the NOE data are used. It becomes, however, organized in two different conformations after energy minimization, which means that this stretch could be in conformational exchange between both conformations (essentially residues 15 and 16) (Figure 4). The two conformations seemed, however, be in fast exchange, regarding the shape of the peaks in the NMR spectra; i.e., no double peaks are observed. In the related toxin ω-conotoxin MVIIA, the corresponding loop was first described as the most flexible part of the molecule (*16, 17*), then in conformational exchange (*18*). Such a conformational exchange has been recently revisited by ^{13}C relaxation analysis and essentially confirmed (*19*).

Of the 34 residues of Ptu1, only the side chains of Cys residues are buried. All side chain conformations are well determined with the exception of the region of the N-terminus (from residues 1 to 4).

Comparison with Other Related Toxins. Ptu1 shares the same structural organization with the ω-conotoxins, i.e., the inhibitor cystin knot motif. Since Ptu1 was homologous to ω-conotoxins in its sequence (Figure 5) and disulfide bridge reticulation, the circular dichroism spectra of the synthetic peptides Ptu1, GVIA (an ω-conotoxin from *Conus geographus*), and MVIIA (an ω-conotoxin from *Conus magus*) have been compared (*1*). The results of these CD measurements show that Ptu1, compared to GVIA and MVIIA, had a much lower content of antiparallel β-sheet and higher content of random coil. The structure of Ptu1 is in good agreement with these data; Ptu1 is formed by a double-stranded antiparallel

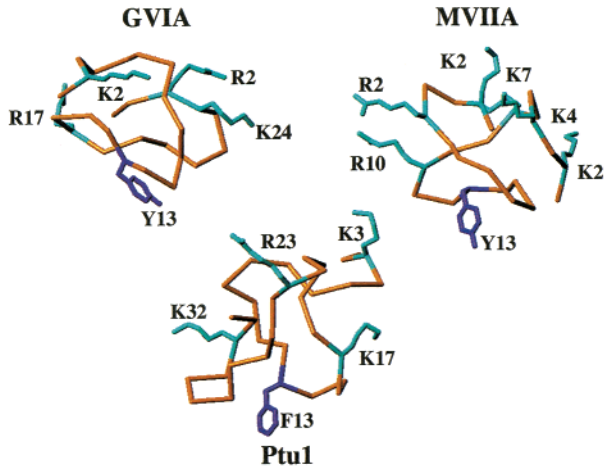

FIGURE 7: Repartition of basic residues (in blue) on the structure of Ptu1 (bottom) and the related toxins GVIA (left) and MVIIA (right). For each structure, the critical aromatic residue is shown in purple.

β-sheet, whereas GVIA and MVIIA possess a triple-stranded β-sheet (Figure 6). The lack of the third strand (encompassing residues 6, 7, and 8 in MVIIA) can easily be explained by the presence of residues that do not allow the stabilization of a β-strand: two prolines (Pro8 and -11) and one glycine (Gly9).

The structure−function relationships of ω-conotoxins GVIA and MVIIA have been previously analyzed (*20*−*22*). Nadasdi et al. (*22*) found that the phenolic group of Tyr13 strongly contributes to the binding affinity of MVIIA, as does the Leu11 side-chain (although a Thr at this position is also tolerated). In addition, substitution of Tyr13 with Phe showed reduction of the affinity of GVIA, indicating that the hydroxyl group of Tyr13 is critical for binding (*23*). Also, the relative contribution of the individual positive charges to N-type voltage-sensitive calcium channel inhibition in MVIIA has been investigated using alanine scanning or, in the case of the N-terminus, N-acetylation (*22*). The results show that the order of importance is Lys2 > Arg10 > N-terminus > Arg21 > Lys7 > Lys4 > Lys24. These residues are shown in Figure 7 in which basic residues are located laterally to the critical tyrosine. Feng et al. (*24*) have demonstrated that mutating Glu1332 belonging to the large extracellular loop between III_{S5} and III_{H5} segments of the N-type calcium channel induced a dramatic slowing of the time course of development of GVIA and MVIIA blocks. Furthermore, Ellinor et al. (*25*) proposed that MVIIA and GVIA block the N-type calcium channel by physically occluding the pore of the channel. Therefore, the complex between MVIIA or GVIA toxins and N-type calcium channel involves a central aromatic residue and lateral basic residues that make salt bridges with Glu1332 but also Glu1334 and Glu1337 (Figure 7).

Ptu1 shares the same pharmacological specificity with MVIIA and GVIA and should therefore present the same

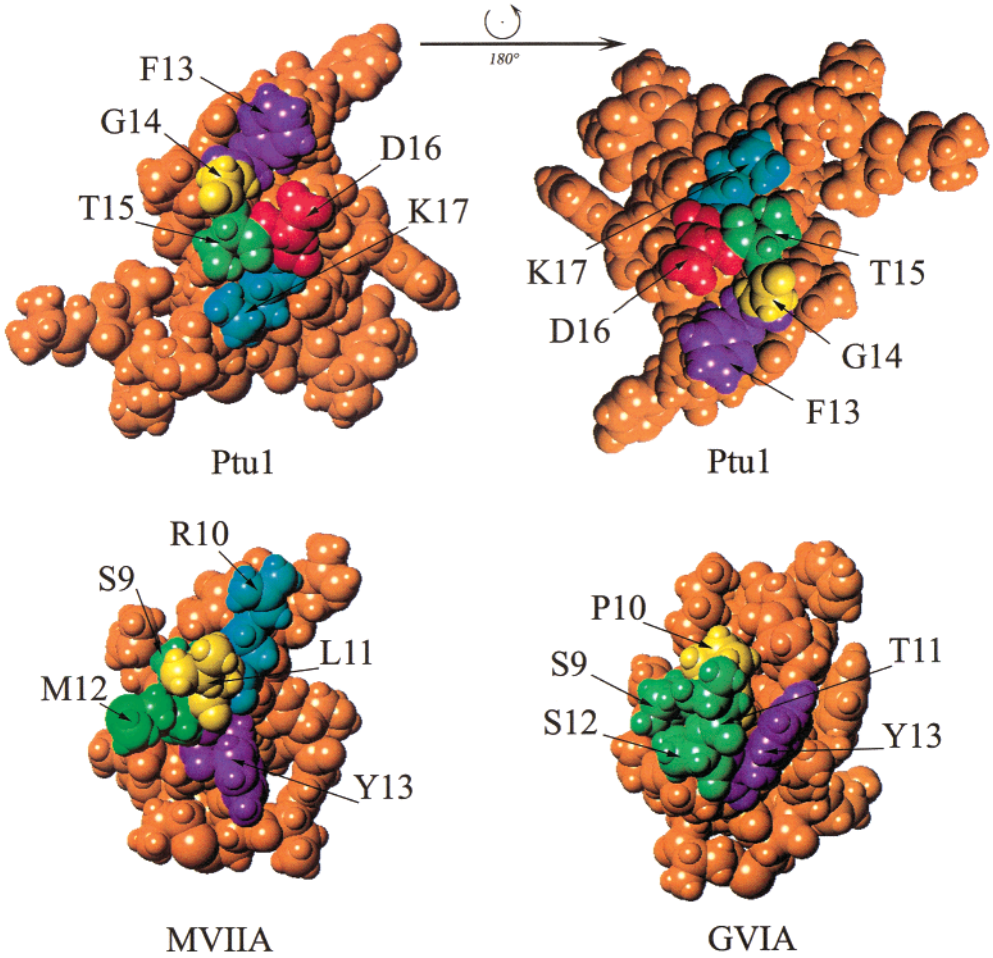

FIGURE 8: CPK representation of Ptu1, MVIIA, and GVIA. The residues of loop 2 are colored according to their side chain type (basic in blue, acidic in red, aliphatic in yellow, aromatic in purple, Met, Thr, and Ser in green) and labeled. The right view of Ptu1 is obtained by a 180° rotation in the plane of the sheet.

type of interacting surface, i.e., encompassing an aromatic residue surrounded by basic residues (primarily Lys2 and Arg10 but also Arg21 and Lys4). Such an organization is found in Ptu1, in which the aromatic residue is Phe13, and the basic residues are Lys17 and Lys32. Therefore, one can conclude that MVIIA, GVIA, and Ptu1 share the same surface of interaction with their common receptor. However, these residues are not in homologous positions when aligning the amino acid sequences (Figure 5): Tyr13 of MVIIA is at the end of loop 2 while Phe13 of Ptu1 is at the beginning of the same loop 2. Thus, to compare the structural features that describe the interacting surface of Ptu1, i.e., loop 2, one has to rotate the structure as shown in Figure 8.

The major difference between Ptu1 and MVIIA loops 2 is the presence of an acidic residue (Asp16) in Ptu1 whose presence could be unfavorable for the binding of Ptu1 on the channel and therefore explain the lower affinity of Ptu1 toward the N-type calcium channel compared to the one of MVIIA.

CONCLUSION

Comparison of the structure of Ptu1 with related N-type calcium channel blockers (MVIIA and GVIA) indicates that a common functional motif can be supported by a common three-dimensional structure but without sequence homology. Mutants of Ptu1 are being developed that will help us to check for the importance of Phe13 and the basic residues for the activity of the toxin.

ACKNOWLEDGMENT

We thank Olivier Bornet for NMR spectral acquisitions and Christian Cambillau for constant help and support.

REFERENCES

1. Corzo, G., Adachi-Akahane, S., Nagao, T., Kusui, Y., and Nakajima, T. (2001) Novel peptides from assassin bugs (Hemiptera:Reduviidae): isolation, chemical and biological characterizations. *FEBS Lett. 497*, 1−6.
2. Marion, D., Ikuto Tschudin, M., and Bax, A. (1989) Rapid recording of 2D NMR spectra without phase cycling. Application to the study of hydrogen exchange in protein. *J. Magn. Reson. 85*, 393−399.
3. Marion, D., and Wüthrich, K. (1983) Application of phase sensitive two-dimensional correlated spectroscopy (COSY) for measurements of H−H spin−spin coupling constants in proteins. *Biochem. Biophys. Res. Commun. 113*, 967−974.
4. Kumar, A., Ernst, R. R., and Wüthrich, K. (1981) A two-dimensional nuclear Overhauser enhancement (2D nOe) experiment for the elucidation of complete proton−proton cross-relaxation networks in biological macromolecules. *Biochem. Biophys. Res. Commun. 95*, 1−6.
5. Piotto, M., Saudek, V., and Sklenar, V. (1992) Gradient-tailored excitation for single-quantum NMR spectroscopy of aqueous solutions. *J. Biomol. NMR 2*, 661−665
6. Sklenar, V., Piotto, M., Leppik, R., and Saudek, V. (1992) Gradient-tailored water suppression for ^{1}H-^{15}N HSQC experiments optimised to retain full sensitivity. *J. Magn. Reson. 102*, 241−245.
7. Bax, A., and Davis, D. G. (1995) MLEV-17-based two-dimensional homonuclear magnetization transfer spectroscopy. *J. Magn. Reson. 65*, 355−360.
8. Griesinger, C., Otting, G., Wüthrich, K., and Ernst, R. R. (1988) Clean-TOCSY for ^{1}H spin system identification in macromolecules. *J. Am. Chem. Soc. 110*, 7870−7872.
9. Wüthrich, K. (1986) in *NMR of Proteins and Nucleic Acids*, John Wiley and sons, New York.
10. Bartels, Ch., Xia, T.-H., Billeter, M., Güntert, P., and Wüthrich, K. (1995) The program XEASY for computer-supported NMR spectral analysis of biological macromolecules. *J. Biomol. NMR 5*, 1−10.
11. Güntert, P., and Wüthrich, K. (1991) Improved efficiency of protein structure calculations from NMR data using the program DIANA with redundant dihedral angle constraints. *J. Biomol. NMR 1*, 447−456.
12. Szyperski, T., Güntert, P., Otting, G., and Wüthrich, K. (1992) Determination of scalar coupling constants by inverse Fourier transformation of in-phase multiplets. *J. Magn. Reson. 99*, 552−560.
13. Laskowski et al. (1993)
14. Bernard, C., Legros, C., Ferrat, G., Bischoff, U., Marquardt, A., Pongs, O., and Darbon, H. (2000) Solution structure of hpTX2, a toxin from Heteropoda venatoria spider that blocks Kv4.2 potassium channel. *Protein Sci. 11*, 2059−2067.
15. Mosbah, A., Kharrat, R., Fajloun, Z., Renisio, J. G., Blanc, E., Sabatier, J. M., El Ayeb, M., and Darbon, H. (2000) A new fold in the scorpion toxin family, associated with an activity on a ryanodine-sensitive calcium channel. *Proteins: Struct., Funct., Genet. 40*, 436−442.
16. Basus, V. J., Nadasdi, L., Ramachandran, J., and Miljanich, G. P. (1995) Solution structure of omega-conotoxin MVIIA using 2D NMR spectroscopy. *FEBS Lett. 370* (3), 163−169
17. Kohno, T., Kim, J. I., Kobayashi, K., Kodera, Y., Maeda, T., and Sato, K. (1995) Three-dimensional structure in solution of the calcium channel blocker omega-conotoxin MVIIA. *Biochemistry 34* (32), 10256−10265.
18. Nielsen, K. J., Thomas, L., Lewis, R. J., Alewood, P. F., and Craik, D. J. (1996) A consensus structure for omega-conotoxins with different selectivities for voltage-sensitive calcium channel subtypes: comparison of MVIIA, SVIB and SNX-202. *J. Mol. Biol. 263* (2), 297−310.
19. Atkinson, R. A., Kieffer, B., Dejaegere, A., Sirockin, F., and Lefevre, J. F. (2000) Structural and dynamic characterization of omega-conotoxin MVIIA: the binding loop exhibits slow conformational exchange. *Biochemistry 39* (14), 3908−3919.
20. Lew, M. J., Flinn, J. P., Pallaghy, P. K., Murphy, R., Whorlow, S. L., Wright, C. E., Norton, R. S., and Angus, J. A. (1997) Structure−function relationships of omega-conotoxin GVIA. *J. Biol. Chem. 272* (18), 12014−12023.
21. Flinn, J. P., Pallaghy, P. K., Lew, M. J., Murphy, R., Angus, J. A., and Norton, R. S. (1999) Roles of key functional groups in w-conotoxin GVIA. *Eur. J. Biochem. 262*, 447−455.
22. Nadasdi, L., Yamashiro, D., Chung, D., Tarczy-Hornoch, K., Adriaenssens, P., and Ramachandran, J. (1995) Structure−Activity analysis of a conus peptide blocker of N-type neuronal calcium channel. *Biochemistry 34* (25), 8076−8081.
23. Kim, J. I., Takahashi, M., Ogura, A., Kohno, T., Kudo, Y., and Sato, K. (1994) Hydroxyl group of tyr 13 is essential for the activity of omega-conotoxin GVIA, a peptide toxin for N-type calcium channel. *J. Biol. Chem. 269* (39), 23876−23878.
24. Feng, Z. P., Hamid, J., Doering, C., Bosey, G. M., Snutch, T. P., and Zamponi, G. W. (2001) Residue G1326 of the N-type calcium channel α_{1B} subunit controls reversibility of ω-conotoxin GVIA and MVIIA block. *J. Biol. Chem*., Feb 2 (epub ahead of print).
25. Ellinor, P. T., Zhang, J. F., Horne, W. A., and Tsien, R. W. (1994) Structural determinants of the blockade of N-type calcium channels by a peptide neurotoxin. *Nature 372*, 272−275.
26. Kraulis, P. J. (1991) MOLSCRIPT: A Program to Produce Both Detailed and Schematic Plots of Protein Structures. *J. Appl. Crystallogr. 24*, 946−950.

BI015537J